J Comput Neurosci
DOI 10.1007/s10827-006-0005-7

Contributions of I_h to feature selectivity in layer II stellate cells of the entorhinal cortex

Julie S. Haas · Alan D. Dorval II · John A. White

Received: 11 January 2006 / Revised: 27 April 2006 / Accepted: 17 July 2006

Abstract Stellate cells (SCs) of the entorhinal cortex generate prominent subthreshold oscillations that are believed to be important contributors to the hippocampal theta rhythm. The slow inward rectifier I_h is expressed prominently in SCs and has been suggested to be a dominant factor in their integrative properties. We studied the input-output relationships in stellate cells (SCs) of the entorhinal cortex, both in control conditions and in the presence of the I_h antagonist ZD7288. Our results show that I_h is responsible for SCs' subthreshold resonance, and contributes to enhanced spiking reliability to theta-rich stimuli. However, SCs still exhibit other traits of rhythmicity, such as subthreshold oscillations, under I_h blockade. To clarify the effects of I_h on SC spiking, we used a generalized form of principal component analysis to show that SCs select particular features with relevant temporal signatures from stimuli. The spike-selected mix of those features varies with the frequency content of the stimulus, emphasizing the inherent nonlinearity of SC responses. A number of controls confirmed that this selectivity represents a stimulus-induced change in the cellular input-output relationship rather than an artifact of the analysis technique. Sensitivity to slow features remained statistically significant in ZD7288. However, with I_h blocked, slow stimulus features were less predictive of spikes and spikes conveyed less information about the stimulus over long time scales. Together, these results suggest that I_h is an important contributor to the input-output relationships expressed by SCs, but that other factors in SCs also contribute to subthreshold oscillations and nonlinear selectivity to slow features.

Keywords Inward rectifier · Reliability · Information theory · Spike-triggered covariance · Principal component analysis · Single-neuron computation

Action Editor: Xiao-Jing Wang

J. S. Haas · A. D. Dorval II · J. A. White (✉)
Department of Biomedical Engineering, Center for BioDynamics, Center for Memory and Brain, Boston University, Boston, MA 02215, USA
e-mail: jwhite@bu.edu

Present address
J. S. Haas
Institute for Nonlinear Science, MC0402, University of California, San Diego, La Jolla, CA 92093-0402, USA

Present address
A. D. Dorval II
Department of Biomedical Engineering, Duke University, 136 Hudson Hall, Box 90281, Durham, NC 27708-0281

Introduction

The parahippocampal region is well known as a formation central to the neural processes of learning and memory. Within this region, the entorhinal cortex (EC) delivers input from the neocortex to the hippocampus proper. Incoming information is carried largely by layer II spiny stellate cells (SCs) of the EC, whose axons deliver the excitatory perforant path input to the hippocampus. The electrophysiological properties of SCs are distinguished by 4–12 Hz subthreshold membrane potential oscillations in response to small, constant-current stimuli (Alonso and Llinás, 1989; Alonso and Klink, 1993). With increasing input current, occasional action potentials arise, phase-locked to the underlying subthreshold oscillations. Because of these intrinsically rhythmic properties, SCs are thought to be major contributors to the theta rhythm, a 4–12 Hz EEG rhythm posited to be important for learning and memory in the hippocampus (Buzsáki, 2002; Hasselmo et al., 2002). Rhythmic behavior in SCs is thought to arise mainly from interactions between

a prominent persistent (noninactivating) Na^+ current and the slow hyperpolarization-activated cation current I_h (Dickson et al., 2000; Klink and Alonso, 1993).

The oscillatory nature of SCs makes them unlikely to serve as simple relay neurons; the nonlinear membrane mechanisms responsible for oscillations are likely to transform the information that SCs pass to the hippocampus. A number of recent studies have examined how the input-properties of SCs and other rhythmic neurons change with the frequency content of the stimulus. One major thread of this work has concentrated on the link between subthreshold oscillations, subthreshold resonance, and frequency-dependent sensitivity to current-clamp stimuli. To a first approximation, these properties can be linked in SCs using linear systems theory (Hutcheon and Yarom, 2000; Schreiber et al., 2004), although this approach breaks down under conditions of significant subthreshold nonlinearity (Haas and White, 2002). Conductance-based models confirm that the relationship between subthreshold resonance and spiking response is subtle and subject to nonlinearities of stochastic and resonant neurons (Richardson et al., 2003).

A second major thread of recent work has focused on the relationship between reliability (repeatability) of stochastic neuronal responses and stimulus frequency content. For stimuli of moderate amplitude, neurons respond most reliably when the frequency content of the stimulus matches the average spiking rate of the neuron (Fellous et al., 2001, Haas and White, 2002; Hunter and Milton, 2003; Hunter et al., 1998; Jensen, 1998). In most cases, the optimal stimulus frequency shifts with depolarization-induced changes in average firing rate; for SCs and other cases, intrinsic membrane mechanisms constrain this optimal frequency to the 4–12 Hz band (Haas and White, 2002; Schreiber et al., 2004).

In this work, we focus on the contribution of the slow inward rectifier I_h to the integrative properties of SCs. We show that blocking I_h with the antagonist ZD7288 eliminates subthreshold resonance, and abolishes the tendency of SCs to respond more reliably to stimuli that are mostly constrained to the 4–12 Hz band. Further, we use generalized principal component analysis (GPCA; Aguera y Arcas and Fairhall, 2003; Brenner et al., 2000), information theoretic techniques, and 'feature detection' models, to reveal a form of feature selectivity in SCs. These detailed analyses show that the selectivity of SCs changes in response to varying temporal structure of the input, on a time scale of seconds. SCs detect slow stimulus features that are likely to be abundant *in vivo* (O'Keefe and Recce, 1993; Raghavachari et al., 2001). Our analyses show that I_h is a contributor to these phenomena, but that other slow response properties of SCs remain in the absence of I_h.

Methods

Electrophysiology

All experiments were conducted as approved by the Boston University Institutional Animal Care and Use Committee. Young (14–35 day old) Long-Evans rats were anesthetized by overexposure to CO_2 and decapitated. The brain was quickly removed and immersed in cold (°C) oxygenated artificial cerebral spinal fluid (ACSF) (in mM: NaCl 126, KCl 3, NaH_2PO_4 1.25, $MgSO_4$ 2, $NaHCO_3$ 26, Glucose 10, $CaCl_2$ 2, buffered to pH 7.4 with 95/5% O_2/CO_2). Horizontal slices were prepared using a Vibratome cutter (TPI). Slices were allowed to recover for 1 h prior to recording in a holding chamber at room temperature, continuously bathed in oxygenated ACSF. The recording chamber was a Haas top (Harvard Apparatus), maintained at 34°C (TC-202A, Harvard Apparatus). Layer II of the EC was visualized by transillumination of the recording chamber. Electrodes of resistance 70–90 MΩ were pulled on a horizontal puller (Sutter Instruments) and filled with 2 M KCl or potassium acetate. Intracellular voltages were amplified (Axoclamp 2B, Axon Instruments), lowpass filtered (lab-made 8-pole Butterworth, cutoff frequency = 5 kHz), and digitized at 10 kHz via software created in LabView (National Instruments) controlling a dedicated-processor I/O board (DAP3200a, Microstar Laboratories) or a LabVIEW DAQ card (PCI-6035E). In most experiments, ionotropic synaptic transmission was blocked by CNQX (10 μM), bicuculline methiodide (10 μM) and AP-5 (30 μM), obtained from Sigma (St. Louis, MO). Even without synaptic blockers, spontaneous synaptic events were too rare and too small to change any of our results. In some experiments, we blocked I_h by adding 100 μM ZD7288 (Tocris-Cookson) to the recording bath solution, in 100 μM concentration (Dickson et al., 2000). ZD7288 has been reported to have effects on membrane mechanisms other than I_h, but none of the known nonspecific effects apply for our experiments. We operated below the concentration (0.5 mM) at which ZD7288 changes the shapes of action potentials (Adachi et al., 2005), and saw no changes in action potentials. ZD7288 can affect synaptic depression (Chevaleyre and Castillo, 2002), but our experiments were done in the presence of synaptic blockers and focused solely on intrinsic cellular properties.

We selected SCs by their superficial position within the EC, and the unique characteristics of their electrophysiological responses to long current steps: a prominent (>25%) sag in response to both depolarizing and hyperpolarizing currents, as well as an early first spike (e.g., Fig. 1(A)) in response to suprathreshold stimuli (Alonso and Klink, 1993; Klink and Alonso, 1993). To each cell, we presented fluctuating current signals with varied frequency content ("frozen

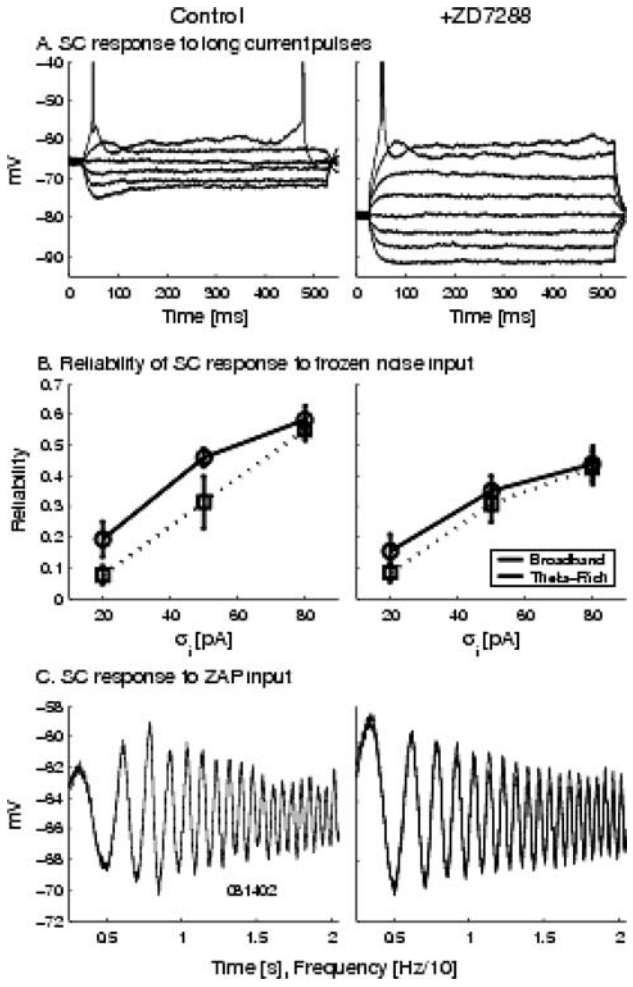

Fig. 1 SC response features depend on I_h. (A) responses of a typical SC to long steps of hyperpolarizing and depolarizing DC current injections (500 ms duration, in steps of 100 pA). With Ih blocked by ZD7288 (right panel), the 'sag' in membrane response is eliminated. (B) In response to multiple presentations of frozen-noise inputs of varying size (see text), the dependence of spiking reliability on input frequency content is reduced in ZD7288 ($N = 9, p < .001$ for control, $p > .05$ for ZD7288, 2-way ANOVA). (C) SCs resonate at theta-range frequencies (left panel, 8 Hz at 0.8 s) in response to subthreshold ZAP stimuli (a uniform-amplitude signal which sweeps through frequencies), but show no such resonance in ZD7288 (right)

noise"; for detail, see Haas and White (2002)). Briefly, the fluctuating current signals were comprised of zero-meaned, lowpass-filtered Gaussian noise signals added to an underlying depolarizing DC pulse. In the present work we focus on responses to two types of lowpass-filtered signals. *Theta-rich* inputs were lowpass filtered with a cutoff frequency of 8 Hz, and had most of their energy focused at theta and lower frequencies. *Broadband* inputs were lowpass filtered at 53 Hz, resulting in a more even distribution of energy across the frequency range of synaptic transmission. A normalization procedure yielded stimuli that were matched in overall amounts of current fluctuation (σ_i, the root-mean-square (RMS) magnitude of the fluctuation) but with different distributions of energy over each frequency band. Each "frozen noise" input was either one or ten seconds in duration, and was delivered between three and ten times per trial, with a long (1–2 s.) rest between repetitions. Trials with different values of σ_i were presented in random order.

Data analysis

Offline analysis was performed using Matlab (Mathworks, Natick, MA). We discarded the first 100 ms of each spike train to eliminate nonstationarities due to spike-rate adaptation, and calculated reliability as the average pairwise cross-correlation, within a 2 ms window of delay, of the point-processes (each convolved with a decaying single exponential with an interaction time constant $\tau_{\text{int}} = 3$ ms) representing the spike trains from each repeated presentation of the stimulus.

Principal component analysis is the transformation between a space populated by a large number of correlated vectors (in this case, spike-triggered inputs), and a space defined by a smaller number of orthogonal vectors (principal components). These components are the eigenvectors of the covariance matrix formed from the original correlated vectors or inputs, and the relative contribution of each component to the variance of the original dataset is indicated by its associated eigenvalue. The general aim of this transformation is to reduce the dimensionality of the original data, by describing the set of inputs by the fewest important eigenvectors that account for the most of the dataset's variance. Under the right conditions, the original dataset can be described as linear combinations of the eigenvectors.

Generalized principal component analysis (GPCA; Aguera y Arcas and Fairhall, 2003; Brenner et al., 2000) operates by the same principles as traditional PCA, but identifies input current components that can potentially combine nonlinearly to elicit spikes. GPCA differs from traditional principal component analysis by the subtraction of another covariance matrix, which restricts the analysis to only the variance common to the spike-triggered stimuli, rather than the overall variance already common to all of the signals. The generalized principal components for SCs were the eigenvectors of the difference-of-covariance matrices Δ_C, where $\Delta_C = C_{spike} - C_{prior}$. In this equation, C_{spike} is the covariance matrix taken from all spike-eliciting stimuli. C_{prior} is a similar matrix, but the input used is triggered randomly from all inputs, rather than triggered on spikes. Subtraction of the covariance matrices reduces the Δ_C to only the spike-triggering fluctuations. Although most of the eigenvalues (Fig. 4) of Δ_C are small, a select few stand apart from the rest, indicating that their corresponding eigenvectors contribute significantly to the spike-eliciting stimuli. To mitigate the effects of autocorrelations within the stimuli themselves, we deconvolved these eigenvectors using a frequency

domain method (Clague et al., 1997). In this method, we took the fast Fourier transform of the eigenvector in question, then divided it by the fast Fourier transform of the filter used to create the frozen noise stimuli on a frequency-by-frequency basis: $\bar{E}_{1,M}(\omega) = E_{1,M}(\omega)/H(\omega)$. We then took inverse fast Fourier transform to obtain the deconvolved eigenvector in the time domain.

Combining Shannon's theory of information transmission (Shannon, 1948) and Bayes' law, we expressed mutual information (Adelman et al., 2003) between a spike train and the driving stimulus as $I = \sum P(stim|spike) \cdot \log_2 \frac{P(stim|spike)}{P(stim)}$.

Using deconvolved versions of the stimuli (Clague et al., 1997), we calculated and plotted mutual information for each point in the 100 ms before the spike (Fig. 6). This analysis indicates the time intervals for which the occurrence of a spike states the most about the information within the stimulus, and, equivalently, which portions of the pre-spike stimulus convey the most information about the occurrence of the spike. We included this analysis as an independent demonstration that SCs integrate their inputs over long time scales, but in a manner that depends on the frequency content and amplitude of the stimulus.

Results

Reliability and resonance properties: Effects of blocking I_h

Bath application of the I_h blocking agent ZD7288 is known to induce significant changes in the membrane responses of SCs (Dickson et al., 2000). Figure 1(A) shows the characteristic response of an SC to long current pulses in both control and blocked conditions; along with the obliteration of the typical 'sag' in response to hyperpolarizing inputs (for the cell shown, 29% in control conditions, 1.9% in ZD7288), bath application of ZD7288 (right panel) also lowered resting membrane potential (in Fig. 1(A) by 13 mV), and raised input resistance (from 35 to 42 MΩ here, though typically the difference was larger). These changes are consistent with results from previous studies (Dickson et al., 2000).

We explored the degree to which ZD7288 affects reliability and resonance in SCs. Figure 1(B) shows plots of spiking reliability vs. RMS current level (σ_i) for broad-band stimuli (cutoff frequency = 53 Hz) and 'theta-rich' stimuli (cutoff frequency = 8 Hz, implying that a larger proportion of the power lies in the 4–12 Hz band). Under control conditions, SCs spike more reliably for theta-rich stimuli (Fig. 1(B), left column, $p < 0.001$ for effect of frequency content on reliability, 2-way ANOVA), as described in our previous work (Haas and White, 2002). Blocking I_h with ZD7288 reduces overall reliability and, especially, the enhancement of reliability for theta-rich stimuli. Under ZD7288, reliability no longer depends on frequency content of input ($p > 0.05$, 2-way ANOVA). ZD7288 also obliterates subthreshold resonance, as determined from responses to uniform-amplitude, frequency-modulated 'ZAP' stimuli, in which frequency sweeps from low to high values linearly in time (Fig. 1(C)). In control conditions, responses to ZAP functions are non-monotonic and show a clear peak at theta frequencies (in Fig. 1(C), near 6 Hz); in ZD7288, responses decrease monotonically.

SCs are well-documented intrinsic oscillators (Alonso and Llinás, 1989; Alonso and Klink, 1993). I_h is poised by its activation curves to take part in SCs' subthreshold rhythmicity, and to add a nonlinear component to any peri-rest integration. Indeed, other groups have reported that in bath application of ZD7288, subthreshold oscillations disappeared from the range of SC behaviors (Dickson et al., 2000). However, for 5 of 5 cells in which we looked specifically for oscillations, theta-range subthreshold oscillations persisted 30 min after application of ZD7288. To quantify oscillatory activity, we defined the *oscillation index* OI as the ratio of power in the 4–10 Hz frequency band to the power in the 10–16 Hz band. For these five cells, which showed no I_h-induced 'sag' or resonance, OI = 2.4 ± 0.2 (mean ± SEM) at depolarized values of voltage (∼ − 50 mV). OI = 1.5 ± 0.2 at hyperpolarized potentials for these cells (∼ − 65 mV). Examples of these subthreshold oscillations from two SCs (each recorded after more than 30 min in bath application of ZD7288) along with autocorrelations and FFTs of the oscillatory activity are shown in Fig. 2, along with a set of oscillations from an SC in control conditions (Fig. 2(E)). These data indicate that I_h may not be the sole slow influence in SC oscillation and integration.

Spike-triggered averages

Our next goal was to assess stimulus selectivity in SCs and its dependence on I_h. The simplest method of evaluation is to calculate the average stimulus preceding a spike. This quantity, the spike-triggered average (STA), is closely related to the optimal linear description of subthreshold processing in neurons (Dayan and Abbott, 2001). For both broad-band (thick black line) and theta-rich (thick gray line) stimuli, STAs recorded in control ACSF include a predictable, sharp upswing in current in the 30 ms preceding a spike (Fig. 3(A)). For theta-rich stimuli, in particular, the STA also includes long and slow hyperpolarizing component for the preceding 70 ms (i.e., $t = -100$ to -30 ms). A two-way analysis of variance (ANOVA) performed on two periods (-15 to -10 ms and -80 to -75 ms) shows that the STA is significantly different for theta-rich and broad-band stimuli ($p < 0.02$), even when the STA is deconvolved to remove inherent stimulus correlations.

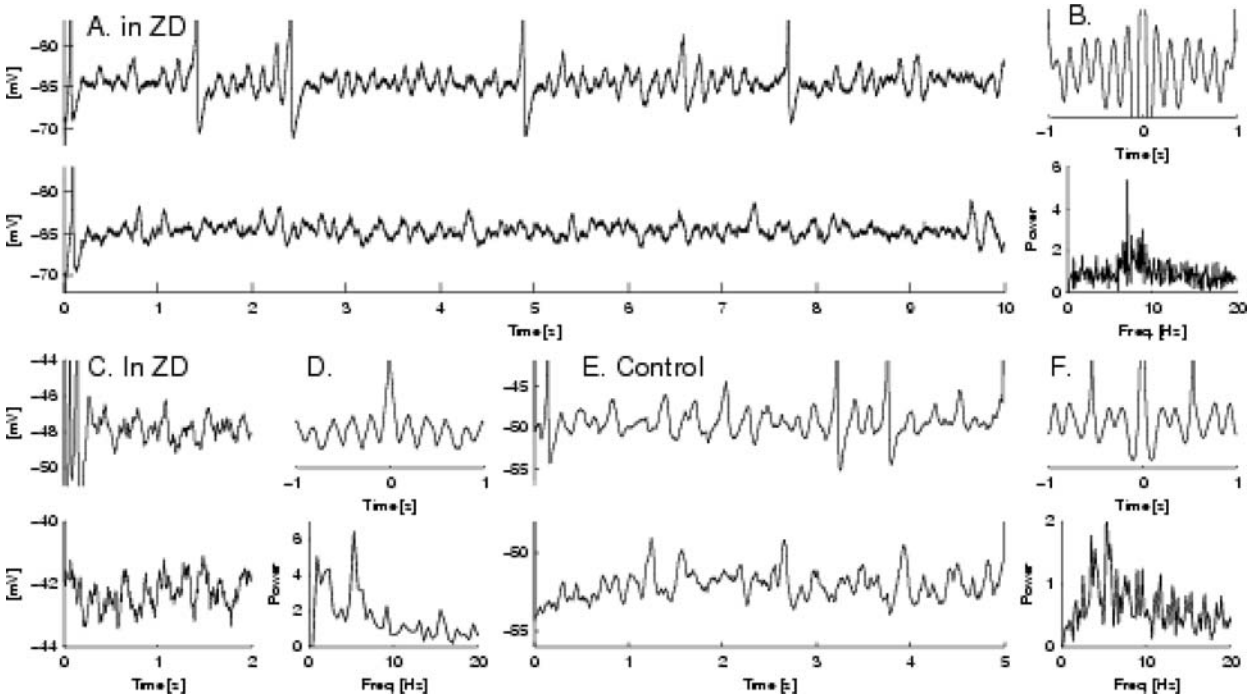

Fig. 2 Subthreshold oscillations persist after I_h is blocked by ZD7288. (A, C, E) Examples of theta-range perithreshold membrane potential oscillations from three SCs. Two traces are shown from each cell. In A and C, data were recorded at least 30 min after bath application of ZD7288. Complete block of I_h was confirmed by the elimination of the "sag" and of resonance in response to ZAP inputs (as in Fig. 1). Subthreshold oscillations are still evident at relatively hyperpolarized (A) and relatively depolarized (C) potentials. E: Sub- and perithreshold oscillations of an SC in control bath solution. (B, D, F) Autocorrelograms (upper panels) and power spectra (lower panels) of the lower traces in A (for panel B), C (for panel D), and E (for panel F) confirm the presence of 4–8 Hz oscillatory subthreshold activity in the presence of ZD7288

Although a slow component is less clear for broadband stimuli than for theta-rich stimuli, closer inspection of the broadband STA (thick black line) in Fig. 3(A) suggests another way in which SCs temporally select slow events within stimuli. We examined the broadband STA for times both immediately before ($t < 0$) and after ($t > 0$) the spike. The data for $t > 0$ is not caused by or related to the spike it follows; instead, it reflects only the autocorrelations, or the average "speed" of the stimulus, as it falls from a high point. Broadband stimuli fall to their mean value within 10 ms; this short time constant arises from the construction of the broadband stimuli, which are uncorrelated for times greater than 10 ms. The pre-spike STA ($t < 0$) is almost twice as wide as its post-spike counterpart, crossing the mean earlier than 20 ms preceding the spike. The asymmetry of the two traces indicates that SCs select relatively slower events within that generally faster stimulus.

Figure 3(B) shows STAs for both types of inputs, delivered in the presence of ZD7288. One might reasonably hypothesize that ZD7288 should eliminate selectivity for slow stimulus components. However, slow components persist in ZD7288, and there is still a statistically significant difference between STAs generated by broadband and theta-rich stimuli, even when STAs are deconvolved to account for temporal

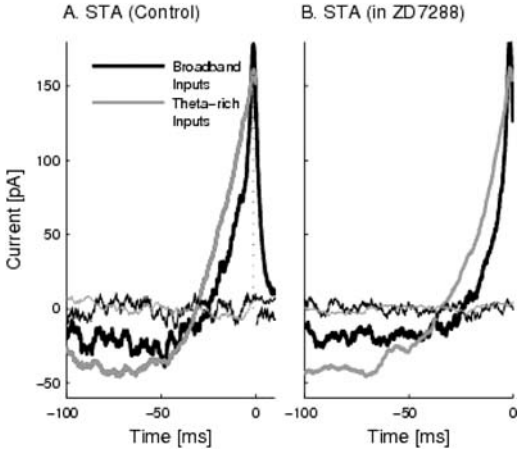

Fig. 3 Spike-triggered averages (STAs) show signs of frequency preference. Thick lines show STAs in response to broadband (black) and theta-rich (gray) inputs. Thin black and gray lines show average traces chosen at randomly triggered times and serve as an internal control. In control conditions (A), both a sharp upswing and a prolonged hyperpolarization, which is more pronounced and structured for theta-rich stimuli, preceded spikes (at $t = 0$). A comparison of the pre- and post-spike time constants of broadband stimuli illustrates a speed-selectivity in SC spiking: from generally fast stimuli (which fall to zero within ~10 ms), SCs spike in response to relatively slower events (which take ~20 ms to rise, also see text). Bath application of ZD7288 (B) does not change STAs a great deal

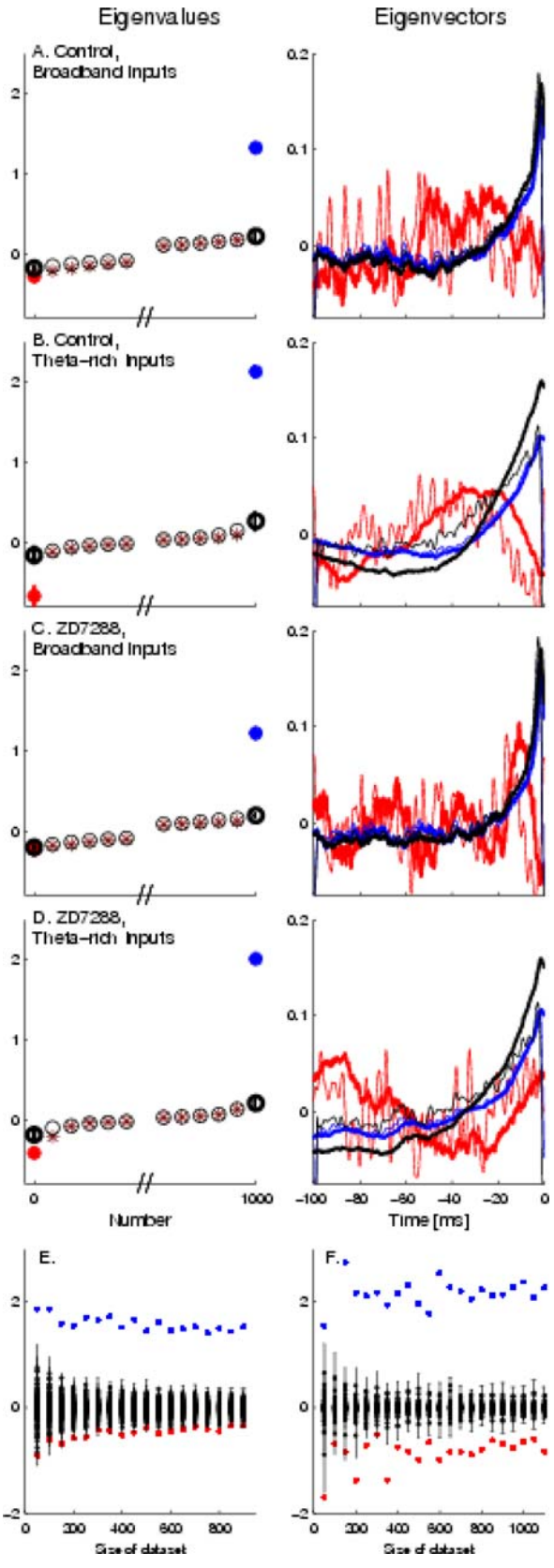

Fig. 4 Results of GPCA reveal a slow component of input underlying SC spiking, in an input-dependent manner. Left plots: eigenvalues of Δ_C (colored symbols), and eigenvalues of shuffled datasets (black circles). For the first and last eigenvalues, error bars (SEM) from five shuffled sets are shown. Right plots: eigenvectors corresponding to the two largest eigenvalues are shown at right; each feature corresponds in color to its associated eigenvalue at left. STAs are shown in black. Thick and thin lines of a given color show raw and deconvolved versions of the eigenvector, respectively. In data collected using broadband inputs (A, C), GPCA only distinguished one significant component of input preceding a spike (blue symbols and lines), which resembled the STA. In data collected using theta-rich inputs (B, D), GPCA revealed two distinct features of input preceding a spike (blue and red symbols and lines). The analysis is robust and significant for our dataset. To ensure that the results were not skewed by the size of the data set, we repeated the analysis using randomly chosen subsets of the data sets under control conditions. For broadband inputs (E), only the STA-like component (blue) was statistically distinguishable from results generated by randomly chosen data sets. For theta-rich inputs (F), two components were statistically distinguishable for most subsets of the data set

correlations in the stimuli ($p < 0.02$, two-way ANOVA on two time windows: -15 to -10 ms and -80 to -75 ms). Although blockade of I_h has clearly changed the STA in Fig. 3(B), we observe that it may still contain slow components, at least for theta-rich stimuli. Because STAs cannot separate different components within a stimulus, and because an STA is limited to a linear description, we study this issue more closely in the next section.

Generalized principal component analysis (GPCA)

While the STA-based analysis in Fig. 3 is reasonable as a general description of SC spike generation, it has a number of shortcomings that we sought to overcome, in order to better understand the SC spiking response. First, STAs as shown may contain confounding effects due to temporal correlations within the non-white stimuli themselves. Second, focusing on the average pre-spike stimulus can mislead intuition for cases in which neurons respond to multiple components of the stimulus, as multiple components are not likely to simply add together to form the STA. Third, our previous observations of nonlinearity of SCs (Haas and White, 2002), as well as the presence of the nonlinear current $I_{h,}$ lead us to expect that the linear STA is insufficient to describe the kernel of SC spiking. To circumvent these issues, we applied generalized principal component analysis (GPCA; see Methods and Aguera y Arcas and Fairhall, 2003; Brenner et al., 2000). We compared GPCA results with STAs that had been deconvolved to remove stimulus correlations.

GPCA uses covariance analysis to select important common features within a set of spike-generating stimuli. Those features are the eigenvectors (Fig. 4, right-hand plots) of a computed matrix, and the contribution of each feature is denoted by its associated eigenvalue (Fig. 4, left-hand plots). In each case, we also performed GPCA on randomly triggered

datasets, as a simple control and a measure of significance; the eigenvalues from that analysis are shown as open circles in each of the left-hand plots, along with error bars representing the standard error of the mean. Important features from spike-triggered data sets should have eigenvalues that stand out from the randomly triggered sets, both graphically in the left-hand panels of Fig. 4 and statistically (e.g., by comparing the largest and smallest eigenvalues from spike-triggered and randomly triggered data sets using a Student's *t*-test).

From broadband stimuli, only one important feature (E_{M}, represented in blue in Fig. 4(A)) was statistically significant at the $p < 0.01$ level. This feature is nearly identical to the STA (cf. blue and black traces in the right-hand panel of Fig. 4(A)). As a reality-check, this similarity is reassuring: the most important common feature among the spike-eliciting stimuli is, simply, the spike-triggered average. These results also imply that only stimulus components in the 25 ms preceding each spike drive the cells reliably for broadband inputs.

From theta-rich stimuli, GPCA revealed two statistically significant components ($p < 0.01$; Fig. 4(B)). The most significant component (E_{M}, blue) again resembles the STA, although not as closely as for the broadband case (cf. the blue and black traces in Fig. 4(B), right-hand panel). The second significant feature (E_1, red) corresponds to neuronal attention over a much longer timescale, indicating that SCs are sensitive to the slow components in theta-rich stimuli.

Two lines of evidence demonstrate that the emergence of the slow component E_1 for theta-rich stimuli is not generated by a change in interspike interval statistics. First, the proportion of interspike intervals in the range 50–100 ms is the same for broadband and theta-rich stimuli (from 11 to 16% for small to large broadband stimuli in both cases). Second, the results are unchanged by omitting spikes that follow interspike intervals < 100 ms.

The differences in feature selectivity between Fig. 4(A) and (B) indicate that SCs change their input-output relationship, or integration, in response to changes in the frequency content of the different stimuli. We are confident that this result is not an artifact of the different statistical structures of broadband and theta-rich stimuli, for a number of reasons. First, the GPCA method itself accounts for common stimulus structure in the construction of the covariance matrix (see Methods). Second, the STAs and features in the right-hand panels of Figs. 3(A)–(B) are shown in both raw and decorrelated form; the decorrelated STAs (light black lines), still differ greatly. Third, as a control, we applied GPCA to subsets of our data, ranging from 10–100% of the entire set. Eigenvalues from this analysis, along with the range of eigenvalues seen from randomly chosen subsets of our data, are plotted in Fig. 4(E)–(F). For this analysis, the STA-like component E_{M} was statistically significant for all subsets in response to both broadband and theta-rich stimuli (Fig. 4(F)). In contrast, the slow component E_1 was never statistically significant for broadband stimuli, but E_1 for theta-rich stimuli was significant for most of stimulus subsets (Fig. 4(E)). GPCA appears to be a robust technique for our dataset.

As a last control, we applied GPCA to theta-rich data following (rather than preceding) SC spikes. This analysis should distinguish stimulus-related correlations from those related to spike generation. As expected, for either broadband or theta-rich stimuli, this analysis only produced one significant eigenvector, which matches the forward-calculated, spike-triggered average (data not shown). Together, our data and controls make us confident that SCs are truly sensitive to the slow component E_1 under these stimulus conditions.

We also applied GPCA to data collected in the presence of ZD7288 (Figs. 4(C)–(D)). Responses to broadband stimuli were much like those recorded under control conditions, with one significant feature that closely resembled the STA (cf. Fig. 4(A)). Responses to theta-rich stimuli in ZD7288 showed a much-reduced, but still statistically significant, contribution of a slow element to SC spiking. Smaller partitions of datasets gathered in ZD7288 gave the same results (data not shown).

Modeling feature detection

Our analysis indicates the slow feature E_1 is statistically significant for theta-rich stimuli in control conditions and in the presence of ZD7288, but that the contribution of E_1 may be smaller in ZD7288. To quantify the contributions of E_{M} and E_1 to the response properties of SCs, we constructed a feature-detection model (Fig. 5(A)). To begin, we cross-correlated the deconvolved versions of both slow and fast features (E_1, E_{M}) with each of the fluctuating-current inputs used in reliability experiments. Peaks of cross-correlations indicated times at which each feature was represented most strongly within an input, and was presumably most likely to elicit a spike. For each cross-correlation, we determined a threshold scaled to the overall amount of fluctuation within the input (σ_i), as $R\sigma_i \cdot R$ was adapted for each input, by matching the number of 'events' predicted by the cross-correlation to the average spike rate produced in SCs by that input. 'Events' were defined as spans of time containing a peak in cross-correlation, above the determined threshold $R\sigma_i$. As such, this model produces an 'event' train, matched in overall rate to the SC spike train, but with responses corresponding solely to a given feature (E_1 or E_{M}).

We measured two outputs from this model. First, from the total number of 'events' predicted by the model, we calculated P_{ev} (dotted lines) as the percentage of those events that corresponded to SC spikes. Second, from the total number of measured SC spikes, we calculated P_{sp} (solid lines) as the percentage of those spikes that corresponded to a predicted 'event' from the model. Results from this analysis are shown

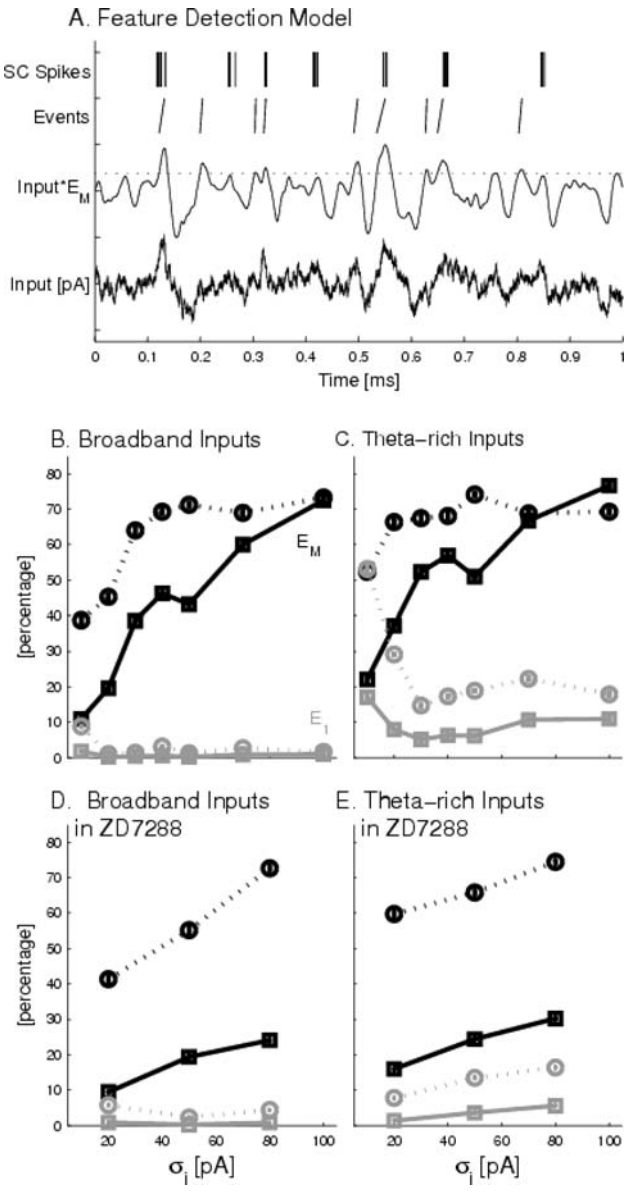

Fig. 5 Results from a feature-detection model. (A) Inputs used in experiments (example, lowest trace) were cross-correlated with each of the two largest features E_M and E_1 from Fig. 4 to create the signals Input*E_M (middle trace) and Input*E_1 (not shown). Thresholding Input*E_M yielded 'events', corresponding to times in the inputs in which the feature was most strongly represented. The resulting 'event' train (bottom raster) is matched in overall rate to the SC spike train (top raster; multiple responses are superimposed) for each input by an adaptive threshold (dashed line). (B, C) P_{ev}, the percentage of 'events' correctly predicted for the inputs used in experiments, are shown by dotted lines and open circles; P_{sp}, the percentage of SC spikes corresponding to a predicted 'event' are solid lines and filled squares. Black lines and symbols correspond to the STA-like component (E_M) from Fig. 4. Gray lines and symbols correspond to the slow component (E_1) from Fig. 4. X axes represent the input RMS power, as in Fig. 1. Only E_M was useful for predicting spikes or events for broadband stimuli. For theta-rich stimuli, the slow feature E_1 was more predictive in control conditions (C) than in ZD7288 (E)

in Figs. 5(B)–(C). For broadband stimuli (Fig. 5(B)), the STA-like feature E_M is a good predictor for both P_{ev} and P_{sp}. Events predict spikes better than spikes predict events. The quality of both predictions increases with increasing stimulus power σ_i. The degree of cross-correlation with the slow feature E_1 is a poor spike predictor for broadband stimuli, independent of stimulus power.

Figure 5(C) shows the same analysis for responses to theta-rich stimuli. In this case, events from correlations of the stimulus with the slow feature E_1 clearly predict spikes with much more fidelity than in the broadband case. Like the results in Fig. 4, this result suggests that the information processing properties of SCs vary, depending on the varying forms of stimuli they receive.

Figures 5(D) and (E) show the analysis extended to data collected in the presence of ZD7288. Results for broadband stimuli are similar to the control case: only E_M contributes to P_{ev} and P_{sp}. For small theta-rich stimuli, the contribution of E_1 to P_{ev} and P_{sp} (gray lines) is significantly diminished (27% and 17% respectively) relative to the control condition ($p < 0.01$, ANOVA, results compared only at the values of σ_i for which we had data under both conditions). Together, results from Figs. 4 and 5 imply that the slow component E_1 is statistically significant but quantitatively less important when I_h is blocked. In addition, ZD7288 increases the discrepancy between P_{ev} and P_{sp} associated with the STA-like component E_M, suggesting that action potential generation is less reliable in the presence of ZD7288. This effect is consistent with the decreased reliability of spiking seen in Fig. 1.

Information theoretic analysis

We considered the time-dependence of mutual information between "whitened" spike-eliciting stimuli (i.e., stimuli that were deconvolved to remove temporal correlations) and the spike train as a function of time before each spike (see Methods). This technique serves as an independent measure of the time duration of integration of SCs, and shows which portions of the features from GPCA are most informative for predicting the timing of subsequent spikes. As shown in Fig. 6(A) and (B), information transfer depends strongly on time, input frequency content and input amplitude. For broadband inputs (Fig. 6(A)), spikes carried information only about the stimulus for the previous 20 ms, corresponding to the width of the peak in the STA (Figs. 3–4). For theta-rich inputs (Fig. 6(B)), spikes carried information about the stimulus over a much longer time scale, as far as 100 ms in the past. The difference in information conveyed by each spike about the stimulus 50–100 ms before the spike was much larger for theta-rich than for broadband stimuli ($p < 10^{-6}$). Qualitatively, history was relatively more important for smaller stimuli: the peak at -75 ms in Fig. 6(B) is higher for small inputs (light gray) than for larger inputs

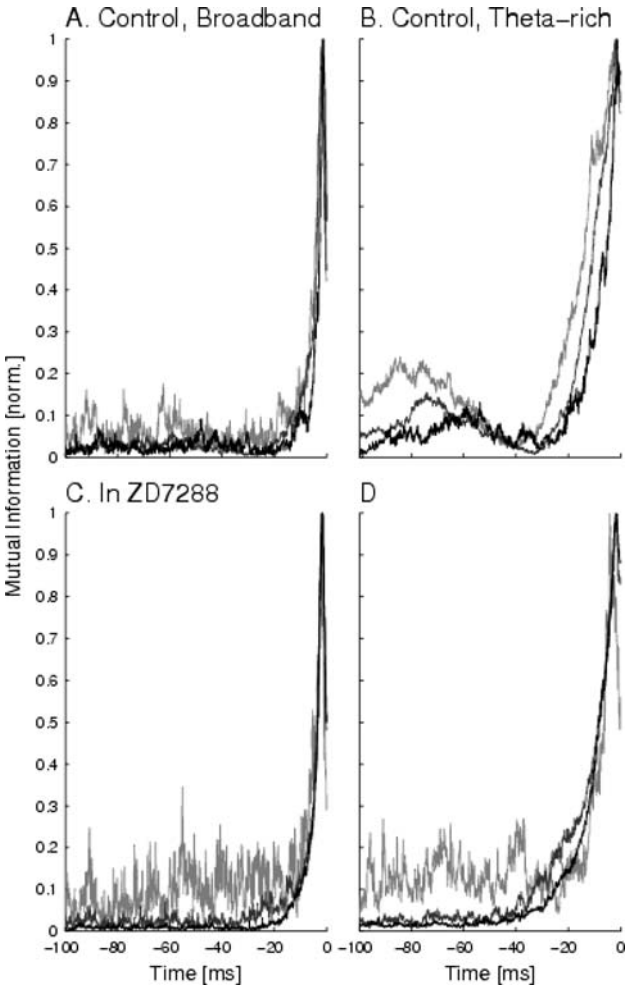

Fig. 6 Information transfer depends on slow processes. (A–D) Mutual information (each trace normalized to its peak) vs. time before the spike reveals temporal dependence of information. Black, dark gray and light gray traces represent responses to stimuli with large, medium, and small fluctuations, respectively. For broadband inputs (A, C), the spike at $t = 0$ carries information about only a very recent history of input. For theta-rich inputs (B, D), spikes carry information about much longer histories of input. The amount of information each spike carries about theta-rich stimuli 50–100 ms in the past is reduced by ZD7288 (see text)

(black; each relative to a normalized maximum of mutual information).

As for our results of feature detection, this result does not appear to be caused by any change in interspike interval statistics (see previous section for details). To a large degree, blocking I_h with ZD7288 removes the temporal structure in information traces, leaving only the peak for 20 ms before the action potential and a noise floor for earlier times, without inducing a noticeable change in interspike interval statistics. In comparison with control conditions, ZD7288 significantly reduced the information conveyed by spikes about the stimulus 50–100 ms before the spike for theta-rich stimuli (2-tailed paired t-test; $p < 10^{-6}$), but did not the conveyed information for broadband stimuli (2-tailed paired t-test; $p > 0.5$). Thus, we can conclude that I_h enhances the information that spikes carry about prior stimuli for theta-rich inputs.

Discussion

Entorhinal stellate cells (SCs) are electrically complex neurons. They display prominent subthreshold oscillations (Alonso and Llinás, 1989; Alonso and Klink, 1993) that reflect, to a large degree, contributions from persistent Na^+ channels and the slow, inward-rectifying cation current I_h (Dickson et al., 2000; Klink and Alonso, 1993). Our goal here was to understand how the inherent rhythmicity of SCs contributes to their properties of signal and information transmission, with particular emphasis on the contributions of I_h. We found that I_h is necessary for subthreshold resonance and frequency-dependent reliability in SCs (Fig. 1), but not necessary for subthreshold oscillations. SCs show highly nonlinear input-output characteristics, in that their spike-triggered averages (Fig. 3) and generalized principal components (Fig. 4) change with the frequency content of the stimulus. Although this nonlinear feature selectivity remains significant with I_h blocked with ZD7288, ZD7288 renders the occurrence of slow stimulus features less predictive of spikes and reduces the amount of information that each spike conveys about the stimulus for the 50–100 ms before the spike. Together, our results indicate that I_h contributes to the slow integrative properties of SCs, but that other factors are at play as well, as indicated by the presence of subthreshold oscillations and slow feature selectivity in the complete block of I_h.

Among our most striking findings was that the information processing capabilities of SCs depend strongly on the nature of the input being received. By responding with different processing filters to differing inputs, SCs are by definition nonlinear integrators. In response to broadband Gaussian stimuli, spike generation was dominated by the STA, confined mainly to the ∼25 ms preceding the spike. In contrast, for theta-rich stimuli, SCs responded significantly to slow components of the stimulus, stretching as far back as 100 ms or more before the spike. We see evidence of this result in simple spike-triggered averages (Fig. 3), and describe it in more detail with GPCA (Fig. 4). Because broadband and theta-rich stimuli were delivered on subsequent trials, in random order with 1 s of rest between trials, we know that this context-dependent sensitivity arises quickly. Our result is reminiscent of *in vivo* data from the fly (Fairhall et al., 2001), in which spike-rate adaptation allows the visual system to transfer high- and low-bandwidth information in an optimal manner. In our case, however, the phenomenon occurs under conditions that do not lead spike-rate adaptation.

ZD7288, a selective blocker of I_h, reduces the importance of this slow component in driving responses of SCs (Fig. 5), implying that I_h plays an important (but not decisive) role in this form of contextual sensitivity in SCs. Without I_h, slow features are still selected, but SCs spike more to random events within input as well (Fig. 5(E)). Those spikes are likely to underlie the reduced detection of a slow feature (Fig. 4(D), and less-robust information transmission (Fig. 6(B)) in ZD7288. Interestingly, in response to inputs like those used in these experiments, a published model of SCs (Acker et al., 2003) does not exhibit similar context sensitivity (data not shown). This result implies that I_h may induce context sensitivity by changing the SCs' response properties on a time scale of seconds. I_h may also work in concert with other nonlinear membrane mechanisms to modulate SCs' sensitivities. This speculated change in properties seems unlikely to be linked to average firing rate or interspike interval patterns, which was largely the same in response to both types of stimulus.

Information theoretic analysis (Fig. 6) suggests that temporal sensitivity depends on stimulus amplitude as well as bandwidth, in that slow components within the stimuli play a more dominant role for stimuli in which the RMS level of fluctuation is small (light-colored lines in Fig. 6). Like the modeling results from Fig. 5, this effect is disrupted substantially by ZD7288.

Although I_h is an important contributor to rhythmicity and feature selectivity, two of our results suggest that SCs express multiple and redundant membrane mechanisms for these purposes. First, in our hands, subthreshold oscillations persisted in 5/5 cells at concentrations of ZD7288 sufficient to block I_h (Fig. 2). This result contrasts with previously published data (Dickson et al., 2000). We hypothesize that methodological differences may underlie this discrepancy (e.g., our animals were 15–35 days old and we recorded via sharp electrodes, whereas Dickson's were 30–60 days old and data was acquired with whole-cell patch). Second, examination of STAs (Figs. 3 and 4) suggests that SCs are still sensitive to slow components within theta-rich stimuli, even with I_h blocked. Under these conditions, the STA (Fig. 3(B)) and the deconvolved STA (thin black line in Fig. 4(D)) indicate sensitivity to stimulus history for around 50 ms preceding the spike, much longer than the 10-ms histories to which neocortical pyramidal cells are most sensitive (Mainen and Sejnowski, 1995). The membrane mechanism responsible for I_h-independent rhythmicity and selectivity to slow components of the stimulus is not known. In CA1 pyramidal cells, both I_h and I_m play separable roles in rhythmic responses (Hu et al., 2002). SCs may be similar to pyramidal cells in this respect. Regardless of the specific mechanisms, redundant mechanisms for subthreshold oscillations and selectivity to slow features is likely to provide greater reliability and flexibility in shaping SC responses to varying inputs.

Given that different levels of vigilance, attention or behavior correspond to major differences in synchrony and EEG patterns (e.g., Fries et al., 1997; Gray et al., 1989; e.g., Niebur et al., 2002; Roelfsema et al., 1997; Singer, 1999; Winson, 1978), the ability of SCs to tailor their responses according to input properties has important repercussions to the parahippocampal network as a whole. In some behavioral states, the parahippocampal region oscillates as a whole at theta or other frequencies (Caplan et al., 2003); in others, no synchronized activity is evident. Because the temporal correlations of inputs to SCs almost certainly varies with behavioral state, we would expect SCs to show behaviorally linked differences in both their reliability (Fig. 1; see also Haas and White, 2002) and in their selectivity for slow stimulus features (Figs. 3–6). This context-sensitive behavior cannot be described adequately using any class of models that assume linear subthreshold behavior and a fixed voltage threshold, because such models necessarily imply feature selectivity that is insensitive to stimulus type (Dayan and Abbott, 2001).

Acknowledgments We owe thanks to the faculty and organizers of the Methods in Computational Neuroscience course at the Marine Biological Lab (Woods Hole, MA, USA), where this project was started. We are particularly grateful to William Bialek, former co-Director of MCN, who provided substantial guidance in use of GPCA and information theoretic methods. We thank Kamal Sen and Jon Shlens for helpful discussions, and Kyle Lillis for reading a preliminary version of the manuscript. This work was supported by grants from the National Institutes of Health (R01 MH61604, R01 NS34425) to J.A. White.

References

Acker CD, Kopell N, White JA (2003) Synchronization of strongly coupled excitatory neurons: Relating network behavior to biophysics. J. Comput. Neurosci. 15: 71–90.

Adachi T, Robinson DM, Miles GB, Funk GD (2005) Noradrenergic modulation of xii motoneuron inspiratory activity does not involve alpha2-receptor inhibition of the ih current or presynaptic glutamate release. J. Appl. Physiol. 98: 1297–1308.

Adelman TL, Bialek W, Olberg RM (2003) The information content of receptive fields. Neuron 40: 823–833.

Aguera Y Arcas B, Fairhall AL (2003) What causes a neuron to spike? Neural. Comput. 15: 1789–1807.

Alonso A, Llinás RR (1989) Subthreshold na + -dependent theta-like rhythmicity in stellate cells of entorhinal cortex layer ii. Nature 342: 175–177.

Alonso A, Klink R (1993) Differential electroresponsiveness of stellate and pyramidal-like cells of medial entorhinal cortex layer ii. J. Neurophysiol. 70: 128–143.

Brenner N, Strong SP, Koberle R, Bialek W, de Ruyter van Steveninck RR (2000) Synergy in a neural code. Neural. Comput. 12: 1531–1552.

Buzsáki G (2002) Theta oscillations in the hippocampus. Neuron 33: 325–340.

Caplan JB, Madsen JR, Schulze-Bonhage A, Aschenbrenner-Scheibe R, Newman EL, Kahana MJ (2003) Human {theta} oscillations

related to sensorimotor integration and spatial learning. J. Neurosci. 23: 4726–4736.

Chevaleyre V, Castillo PE (2002) Assessing the role of ih channels in synaptic transmission and mossy fiber ltp. Proc. Natl. Acad. Sci. USA 99: 9538–9543.

Clague H, Theunissen F, Miller JP (1997) Effects of adaptation on neural coding by primary sensory interneurons in the cricket cercal system. J. Neurophysiol. 77: 207–220.

Dayan P, Abbott LF (2001) Theoretical Neuroscience: Computational and Mathematical Modeling of Neural Systems, Edition. Massachusetts Institute of Technology Press, Cambridge, Mass.

Dickson CT, Magistretti J, Shalinsky MH, Fransen E, Hasselmo ME, Alonso A (2000) Properties and role of i(h) in the pacing of subthreshold oscillations in entorhinal cortex layer ii neurons. J. Neurophysiol. 83: 2562–2579.

Fairhall AL, Lewen GD, Bialek W, de Ruyter Van Steveninck RR (2001) Efficiency and ambiguity in an adaptive neural code. Nature 412: 787–792.

Fellous JM, Houweling AR, Modi RH, Rao RP, Tiesinga PH, Sejnowski TJ (2001) Frequency dependence of spike timing reliability in cortical pyramidal cells and interneurons. J. Neurophysiol. 85: 1782–1787.

Fries P, Roelfsema PR, Engel AK, Konig P, Singer W (1997) Synchronization of oscillatory responses in visual cortex correlates with perception in interocular rivalry. Proc. Natl. Acad. Sci. USA 94: 12699–12704.

Gray CM, Konig P, Engel AK, Singer W (1989) Oscillatory responses in cat visual cortex exhibit inter-columnar synchronization which reflects global stimulus properties. Nature 338: 334–337.

Haas JS, White JA (2002) Frequency selectivity of layer ii stellate cells in the medial entorhinal cortex. J. Neurophysiol. 88: 2422–2429.

Hasselmo ME, Bodelon C, Wyble BP (2002) A proposed function for hippocampal theta rhythm: Separate phases of encoding and retrieval enhance reversal of prior learning. Neural. Comput. 14: 793–817.

Hu H, Vervaeke K, Storm JF (2002) Two forms of electrical resonance at theta frequencies, generated by m-current, h-current and persistent na+ current in rat hippocampal pyramidal cells. J. Physiol. 545: 783–805.

Hunter JD, Milton JG (2003) Amplitude and frequency dependence of spike timing: Implications for dynamic regulation. J. Neurophysiol. 90: 387–394.

Hunter JD, Milton JG, Thomas PJ, Cowan JD (1998) Resonance effect for neural spike time reliability. J. Neurophysiol. 80: 1427–1438.

Hutcheon B, Yarom Y (2000) Resonance, oscillation and the intrinsic frequency preferences of neurons. Trends Neurosci 23:216–222.

Jensen RV (1998) Synchronization of randomly driven nonlinear oscillators. Physiol. Rev. E 58: 6907–6910.

Klink R, Alonso A (1993) Ionic mechanisms for the subthreshold oscillations and differential electroresponsiveness of medial entorhinal cortex layer ii neurons. J. Neurophysiol. 70: 144–157.

Mainen ZF, Sejnowski TJ (1995) Reliability of spike timing in neocortical neurons. Science 268: 1503–1506.

Niebur E, Hsiao SS, Johnson KO (2002) Synchrony: A neuronal mechanism for attentional selection? Curr. Opin. Neurobiol. 12: 190–194.

O'Keefe J, Recce ML (1993) Phase relationship between hippocampal place units and the eeg theta rhythm. Hippocampus 3: 317–330.

Raghavachari S, Kahana MJ, Rizzuto DS, Caplan JB, Kirschen MP, Bourgeois B, Madsen JR, Lisman JE (2001) Gating of human theta oscillations by a working memory task. J. Neurosci. 21: 3175–3183.

Richardson MJ, Brunel N, Hakim V (2003) From subthreshold to firing-rate resonance. J. Neurophysiol. 89: 2538–2554.

Roelfsema PR, Engel AK, Konig P, Singer W (1997) Visuomotor integration is associated with zero time-lag synchronization among cortical areas. Nature 385: 157–161.

Schreiber S, Erchova I, Heinemann U, Herz AV (2004) Subthreshold resonance explains the frequency-dependent integration of periodic as well as random stimuli in the entorhinal cortex. J. Neurophysiol. 92: 408–415.

Schreiber S, Fellous J-M, Tiesinga P, Sejnowski TJ (2004) Influence of ionic conductances on spike timing reliability of cortical neurons for suprathreshold rhythmic inputs. J. Neurophysiol. 91: 194–205.

Shannon CE (1948) A mathematical theory of communication. Bell Syst. Tech. J. 27: 379–423; 623–656.

Singer W (1999) Neurobiology. Striving for coherence [news; comment]. Nature 397: 391–393.

Winson J (1978) Loss of hippocampal theta rhythm results in spatial memory deficit in the rat. Science 201: 160–163.